

## Tomographic reconstruction using 3D deformable models

X L Battle<sup>†</sup>, G S Cunningham<sup>‡</sup> and K M Hanson<sup>§</sup>

MS-P940, Los Alamos National Laboratory, Los Alamos, NM, 87545, USA

Received 31 July 1997

**Abstract.** We address the issue of reconstructing the shape of an object with uniform interior activity from a set of projections. We estimate directly from projection data the position of a triangulated surface describing the boundary of the object while incorporating prior knowledge about the unknown shape. This inverse problem is addressed in a Bayesian framework using the maximum *a posteriori* (MAP) estimate for the reconstruction. The derivatives needed for the gradient-based optimization of the model parameters are obtained using the adjoint differentiation technique. We present results from a numerical simulation of a dynamic cardiac imaging study. A first-pass exam is simulated with a numerical phantom of the right ventricle using the measured system response of the University of Arizona FASTSPECT imager, which consists of 24 detectors. We demonstrate the usefulness of our approach by reconstructing the shape of the ventricle from 10 000 counts. The comparison with an ML-EM result shows the usefulness of the deformable model approach.

### 1. Introduction

The present work represents a natural progression of efforts to use geometric models to perform tomographic reconstruction. These efforts started with the use of simple shapes (Rossi and Willsky 1984) to interpret projection data, which were extended to deal with more complicated three-dimensional shapes (Bresler and Macovski 1987, Bresler *et al* 1989). Deformable models, which are commonly used in medical imaging for tasks such as segmentation and restoration (Staib and Duncan 1996), have also been used to solve ill-posed tomographic reconstruction problems (Hanson 1993a, b, Chiao *et al* 1994). Bayesian methods can substantially improve the accuracy of the reconstructions obtained from limited data by making use of prior knowledge concerning the geometrical shape of the object.

Hanson *et al* (1994), Hanson and Cunningham (1996a, b) and Cunningham *et al* (1994a, b) have developed a framework in which such analysis can be easily conducted. The Bayes inference engine (BIE) is a flexible modelling tool that allows one to interactively define models of radiographic measurement systems and geometric models of objects. Based on an object-oriented design, the BIE allows one to create a measurement model, define a geometric description of the object, and optimize a likelihood or posterior with respect to the user-selected parametrization. This optimization problem would be intractable without the knowledge of the gradient of the posterior. Adjoint differentiation (Hanson and Cunningham 1996a) addresses this issue in a very efficient and elegant way.

<sup>†</sup> Present address: Laboratoire de Biophysique, Université de Bretagne Occidentale, BP 815, 29285 Brest Cedex, France. E-mail address: xavier.battle@univ-brest.fr

<sup>‡</sup> E-mail address: cunning@lanl.gov

<sup>§</sup> Author to whom correspondence should be addressed. E-mail address: kmh@lanl.gov

We illustrate these methods by reconstructing the shape of an object of uniform interior activity from a set of projections. We recall the principles of Bayesian analysis and present the specific characteristics of this 3D problem, as well as the principles of adjoint differentiation. We discuss the choice of an appropriate model and a meaningful prior, as well as the appropriate likelihood function. Based on the results of a numerical simulation, we show the value of this approach in the context of single photon emission computed tomography (SPECT) dynamic cardiac imaging. The results of the reconstructions from simulated first-pass data show the advantages of the method in high-noise situations compared with a reconstruction from a classical activity-based method, specifically the ML-EM algorithm.

## 2. Bayesian approach

The Bayesian method is a model-based approach to analysis in which prior knowledge is integrated with measurements. Given some data  $d$ , the probability of an hypothesis  $x$  is given by Bayes's law:

$$P(x|d) = \frac{P(d|x) P(x)}{P(d)} \quad (1)$$

where  $P(x|d)$  denotes the posterior probability,  $P(d|x)$  the likelihood of the data  $d$  given the hypothesis  $x$ , and  $P(x)$  the prior probability of  $x$ . The denominator  $P(d)$  is the integral of the numerator over  $x$ , which properly normalizes the posterior. The maximum *a posteriori* (MAP) estimate is the value of  $x$  that maximizes  $P(x|d)$ . Maximizing the posterior is equivalent to minimizing the minus-log-posterior function:

$$\varphi(x) = -\ln P(x|d) = -\ln P(d|x) - \ln P(x) + \text{constant} \quad (2)$$

keeping only the terms that depend on the optimized variable  $x$ .

Here we reconstruct the shape of an unknown object from a set of projections. The unknown shape is represented by a geometrical model, which constitutes our hypothesis. The simulation of the measurement process produces the predicted data. The comparison of the predicted data with the actual data gives the likelihood of our hypothesis. Prior knowledge is incorporated as another function of the hypothesis to produce the posterior function. An optimization procedure yields the MAP estimate parameters specifying the surface position. In the following sections we discuss these aspects in more detail.

### 2.1. Object model

We focus on objects of uniform interior activity for which the shape is of interest. We therefore wish to represent the shape of the external surface of the object rather than the full volume. There are numerous ways to represent a 2D surface in 3D space. We choose to represent the objects by a closed, finely divided triangulated surface enclosing a region of uniform activity.

The simplicity of the triangulated surface model has several advantages. By increasing the resolution (by increasing the number of vertices), one can represent almost any surface, even the most contorted. We emphasize that no smoothness constraint is embedded in such a model. From a Bayesian modelling perspective, a representation that is free of constraints is desirable because it allows one to apply constraints explicitly in terms of the prior on the surface (Hanson *et al* 1997a, b).

As an alternative surface description, spline surfaces can represent a smooth surface with relatively few parameters. However, they do so only because their surfaces are controlled

by a fairly strong smoothness constraint. The disadvantage of such descriptions is that they effectively replace the smoothness control on the surface that can be specified with a prior. One is then stuck with only a limited means of altering the smoothness of the surface. Another disadvantage of splines is that the degree of smoothness can only be controlled in a discrete way, for example, by changing the order of the interpolating polynomial (Hanson *et al* 1997b).

The triangulated surface is not only very flexible, but also the simplest kind of surface model. As a consequence, the algorithms developed for this structure remain fairly simple, which is important for adjoint differentiation discussed in section 3.

## 2.2. Likelihood

In nuclear medicine the number of gamma rays detected in each detector pixel generally follow a Poisson probability distribution. However, the likelihood for the corrected data from actual emission scanners is much more complicated than a simple Poisson distribution (Fessler 1994). For the present purposes we choose to use one-half of a weighted chi-squared for the minus-log-likelihood

$$-\ln P(d|x) = \sum_i \frac{(n_i - \hat{n}_i)^2}{2(n_i + 1)} \quad (3)$$

where  $n_i$  is the measured number of counts in the  $i$ th detector pixel and  $\hat{n}_i$  is the expected number (not necessarily an integer). The sum is over all detector pixels. Essentially, we are setting the variance to  $n_i + 1$ , instead of the actual variance of the Poisson distribution,  $\hat{n}_i$ . This expression roughly approximates the Poisson distribution, but more importantly, it can provide a chi-squared approximation for any minus-log-likelihood distribution by adjusting the denominator to match the expected variance. The BIE can handle the Poisson distribution just as well.

The predicted number of counts  $\hat{n}_i$  is obtained by converting the surface description to a voxelated grid in which each voxel value represents its activity. The system projection matrix is then used to calculate the expected number of counts in the gamma-ray detectors.

## 2.3. Prior

The intended application is the reconstruction of the shape of the blood pool within the heart. In dynamic SPECT the magnitude of the noise implied by the small number of counts expected in each time frame will significantly degrade the quality of the projection data. Without regularization the reconstructions are expected to be jagged and spiky. We therefore incorporate prior knowledge about the expected degree of smoothness of the reconstructed shape under the assumption that the walls of the heart are fairly smooth.

A good measure of the smoothness of a continuous curve in two dimensions is given by the integral of the curvature squared along the curve. This integral can be reasonably approximated for a polygon (Hanson *et al* 1996, 1997a, b). The generalization of this approach to surfaces in 3D is not straightforward because of the tensorial nature of the curvature. However, as a first approximation, we use a measure of the smoothness of the triangulated surface based on comparing the directions of normals of neighbouring triangles. The expression we use for the minus-log-prior is

$$-\ln P(x) = \frac{\alpha}{S} \sum_{i \in T} S_i \sum_{j \in N(i)} \tan^2 \left( \frac{\theta_{i,j}}{2} \right) \quad (4)$$

where  $T$  denotes the set of all triangles,  $N(i)$  denotes the set of the neighbours of the triangle of index  $i$ ,  $\theta_{i,j}$  denotes the angle between the normals of triangles of indices  $i$  and  $j$ ,  $S_i$  is the area of the triangle of index  $i$ , and  $S$  is the total surface area. The coefficient  $\alpha$  regulates the strength of the prior relative to the likelihood. Since the MAP solution strikes a balance between the likelihood and the prior,  $\alpha$  has a considerable influence on the MAP reconstruction.

### 3. Adjoint differentiation

#### 3.1. Motivation

The MAP estimate is found by minimizing the minus-log-posterior,  $\varphi$  in equation (2), with respect to the parameters that determine the shape of the object, namely the positions of the vertices of the triangles. For the sake of efficiency, it is desirable to employ gradient-based methods in this minimization. Therefore, the derivatives of  $\varphi$  with respect to the model parameters must be computed. Since the models considered involve many thousands of parameters, a quick way to compute the derivatives of  $\varphi$  with respect to the model parameters is required. Adjoint differentiation addresses this issue in a very efficient way (Hanson and Cunningham 1996a).

#### 3.2. Principle

Consider a sequence of transformations,  $A$ ,  $B$ , and  $C$ , that transform a parameter vector  $x$  into a scalar  $\varphi$ :

$$x \xrightarrow{A} y \xrightarrow{B} z \xrightarrow{C} \varphi \quad (5)$$

where  $y$  and  $z$  are intermediate data structures. One wants to compute the derivatives of  $\varphi$  with respect to the  $x_i$  in a computationally efficient way. The chain rule for differentiation gives the derivatives of  $\varphi$  with respect to  $x_i$ :

$$\frac{\partial \varphi}{\partial x_i} = \sum_{jk} \frac{\partial \varphi}{\partial z_k} \frac{\partial z_k}{\partial y_j} \frac{\partial y_j}{\partial x_i}. \quad (6)$$

The essence of adjoint differentiation is to perform the sum on the indices in equation (6) in the reverse order from that used in the forward calculation. By doing the sum on  $k$  before that on  $j$ , sequence (5) is reversed:

$$I \xrightarrow{C'} \frac{\partial \varphi}{\partial z} \xrightarrow{B'} \frac{\partial \varphi}{\partial y} \xrightarrow{A'} \frac{\partial \varphi}{\partial x} \quad (7)$$

where  $I$  is the identity vector and  $\partial \varphi / \partial \mathbf{y}$  denotes the gradient vector of  $\varphi$  wrt  $\mathbf{y}$ . The intermediate data structures in sequence (7) are vectors, similar to the ones in (5). For each forward transformation, an adjoint counterpart exists.

The details of the implementation of adjoint differentiation for the underlying algorithm required for the present problem may be found in the paper by Battle *et al* (1997).

### 4. Results

To demonstrate the effectiveness of the approach, we reconstruct the shape of a computer model of a right ventricle from numerically simulated data. In the context of a first-pass exam, the radioisotope density in the blood pool in the right ventricle can be considered as

homogeneous. The ventricle can therefore be represented as an object with uniform interior activity. The simulation is based on the University of Arizona FASTSPECT imaging system (Klein *et al* 1995). This system consists of 24 pinhole gamma-ray cameras surrounding the volume being imaged. Each camera has a resolution of 64 by 64 pixels. The system response of the scanner has been measured by moving a source the size of one voxel,  $(2 \text{ mm})^3$ , through the active volume and recording the response of each of the 24 detector planes. The size of the voxel grid is  $40 \times 39 \times 37$ .

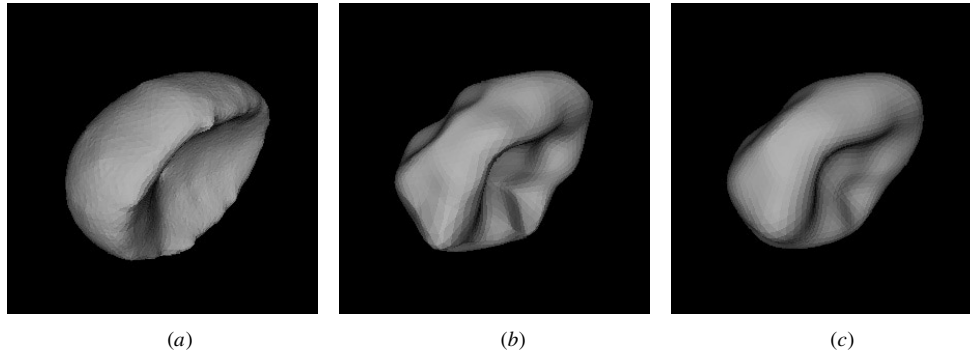


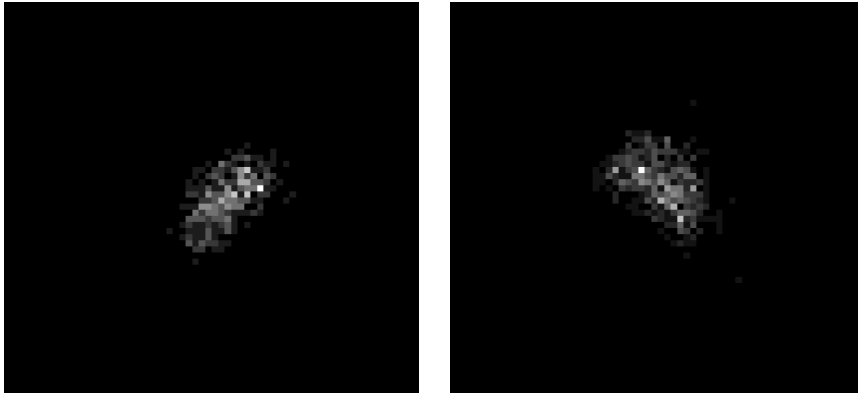
**Figure 1.** The original object, a numerical phantom representing the right ventricle (a) and reconstructions obtained for  $\alpha = 6$  (b) and  $\alpha = 10$  (c).

We use a numerical model of the right ventricle as our object of study. The phantom, shown in figure 1, consists of a very finely triangulated surface containing 30 048 triangles and 15 026 vertices. We simulate a single 50 ms frame from a dynamic study with a total of 10 000 counts in all 24 detectors using a Poisson distribution. Such a low-count situation is expected for a single frame of an actual dynamic first-pass exam. Figure 2 shows two of the 24 projections. The number of counts per pixel varies from 0 to 9, with an average of 0.5. The reconstruction task is to determine the position of the ventricle surface from the measured emission data. The surface determination may be used to estimate the volume of the ventricle. In a dynamic exam, the surface position versus time may provide even more useful diagnostic information concerning cardiac function.

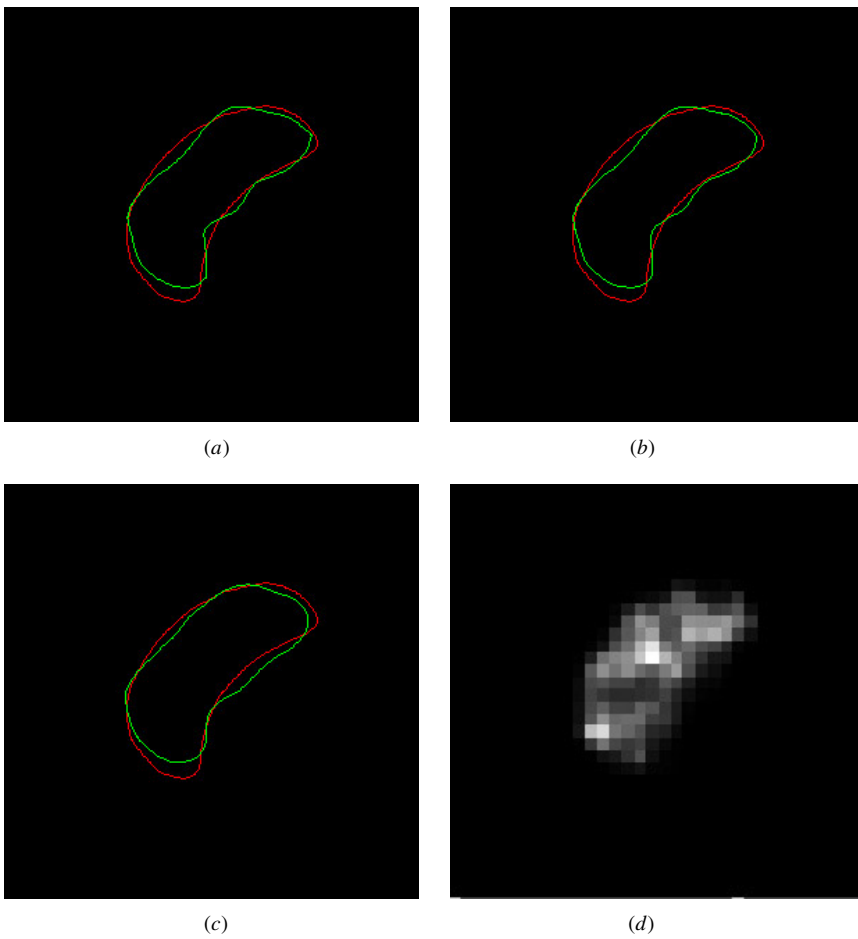
The reconstruction is obtained by deforming a surface to minimize the minus-log-posterior. Starting with a triangulated sphere containing 2562 vertices and 5120 triangles, the positions of the vertices of the triangles and the magnitude of the uniform interior activity are varied. The MAP estimate is obtained in about 50 global iterations (line searches) of a variable metric optimization technique (Dennis and Schnabel 1983). Figure 1 shows reconstructions obtained for various values of  $\alpha$ . Obviously, the choice of  $\alpha$  influences the smoothness of the reconstruction.

Figure 3 shows contours obtained by slicing the phantom and the reconstruction in an arbitrary plane. Again, we notice the influence of the choice of  $\alpha$  on the reconstruction. The maximum error on the position of the surface has approximately the width of a voxel (i.e. 2 mm). The total volume of the reconstructed object for  $\alpha = 8$  is within 6% of that of the original phantom.

Figure 3 also shows a slice through the estimated activity of an ML-EM reconstruction (Shepp and Vardi 1982) after 30 iterations. This ML-EM result compares well visually with our estimated contours. The voxels at the edge of the ventricle in this activity-based reconstruction contain reduced activity. Because of this effect and the rather large size of the voxels, it is difficult to estimate the position of the boundary of the blood pool from this



**Figure 2.** Simulated projection data for two of the 24 detectors.



**Figure 3.** Slices through the original and the reconstructions (wider line) for  $\alpha = 6$  (a),  $\alpha = 8$  (b),  $\alpha = 10$  (c), and the ML-EM reconstruction (d).

ML-EM result. Thus, we find it difficult to make a direct quantitative comparison between our results and those obtained by the conventional ML-EM algorithm. One benefit of our surface representation is that it provides subvoxel localization, although such accuracy is perhaps not achieved in this low-count simulation.

## 5. Discussion

This work illustrates how deformable models can be used to solve ill-posed, three-dimensional tomographic reconstruction problems. The results demonstrate the usefulness of deformable models within the context of the Bayesian approach.

The potential complexity of geometric shapes implies the existence of multiple local minima in the minus-log-posterior functional that we employ here. Therefore, the surface model must be properly initialized to obtain a sensible reconstruction. There are several approaches to overcoming this problem. One approach, applicable to clinical situations, is to start with a generic model that describes an 'average' patient. An alternative general and robust method that works well for relatively simple scenes is to employ a multiresolution optimization. One starts by optimizing the geometric shape at coarse resolution, realized by blurring the intermediate voxel representation. Then one proceeds to optimize at finer and finer resolutions (Cunningham *et al* 1996). In any case, whatever method is employed for overcoming the initialization problem, it must be thoroughly tested on clinical data to verify its efficacy.

Potential complications that might arise in analysing real data include non-uniform interior activity, the presence of activity outside the ventricle, and scatter background. An advantage of our model-based approach is that it can readily accommodate deviations from the simplifying assumptions that we have made in our analysis. For example, if the blood pool activity is non-uniform, our model can be augmented to include non-uniform activities inside the ventricle surface. Similarly, the presence of activity outside the ventricle or contributions from scatter can be handled by extending the model. The flexibility built into the BIE makes it easy to alter the analysis models.

Many issues need further attention. The selection of the strength of the prior is a crucial issue and an automatic selection of it from the data is currently being investigated. A prior penalizing high values of the derivative of the curvature rather than the curvature itself seems desirable. The reconstruction of a real object, such as a CardioWest total artificial heart, from actual data taken at the University of Arizona will better validate the approach. Time-evolving problems will also be addressed in the future.

## Acknowledgments

This work was supported by the US Department of Energy under contract W-7405-ENG-36. We are indebted to Harry Barrett and Don Wilson of the University of Arizona for supplying us their FASTSPECT measurement matrix and a suitable numerical phantom.

## References

- Battle X L, Hanson K M and Cunningham G S 1997 3D Tomographic reconstruction using geometrical models *Proc. SPIE* **3034** 346–57
- Bresler Y, Fessler J A and Macovski A 1989 A Bayesian approach to reconstruction from incomplete projections of a multiple object 3D domain *IEEE Trans. Pattern Analysis Machine Intelligence* **11** 840–58

- Bresler Y and Macovski A 1987 Three-dimensional reconstruction from projections with incomplete and noisy data by object estimation *IEEE Trans. Acoust. Speech Signal Process.* **35** 1139–52
- Chiao P-C, Rogers W L, Fessler J A, Clinthorne N H and Hero A O 1994 Model-based estimation with boundary side information or boundary regularization *IEEE Trans. Med. Imaging* **13** 227–34
- Cunningham G S, Hanson K M, Jennings G R and Wolf D R 1994a An object-oriented implementation of a graphical-programming system *Proc. SPIE* **2167** 914–23
- 1994b An interactive tool for Bayesian inference *Rev. Prog. Quant. Nondestructive Evaluation* **14A** 747–54
- 1994c An object-oriented optimization system *Proc. IEEE Int. Conf. on Image Processing (Austin, TX, 1994)* vol III (Los Alamitos, CA: IEEE Computer Society Press) pp 826–30
- Cunningham G S, Koyfman I and Hanson K M 1996 Improved convergence of gradient-based reconstructions using multi-scale models *Proc. SPIE* **2710** 145–55
- Dennis J E and Schnabel R B 1983 *Numerical Methods for Unconstrained Optimization and Nonlinear Equations* (Englewood Cliffs, NJ: Prentice-Hall) p 213
- Fessler J A 1994 Penalized weighted least-squares image reconstruction for positron emission tomography *IEEE Trans. Med. Imaging* **13** 290–300
- Hanson K M 1993a Bayesian reconstruction based on flexible prior models *J. Opt. Soc. Am.* **10** 997–1004
- 1993b Flexible prior models in Bayesian image analysis *12th Int. Workshop of Maximum Entropy and Bayesian Methods (Paris, 1992)* ed A Mohammad-Djafari and G Demoment (Dordrecht: Kluwer Academic) pp 399–406
- Hanson K M, Bilisoly R L and Cunningham G S 1996 Kinky tomographic reconstruction *Proc. SPIE* **2710** 156–66
- Hanson K M and Cunningham G S 1996a A computational approach to Bayesian inference *Comput. Sci. Stat.* **27** 202–11
- 1996b The Bayes inference engine *15th Int. Workshop of Maximum Entropy and Bayesian Methods (Santa Fe, NM, 1995)* ed K M Hanson and R N Silver (Dordrecht: Kluwer Academic) pp 125–34
- 1995 Exploring the reliability of Bayesian reconstructions *Proc. SPIE* **2434** 416–23
- Hanson K M, Cunningham G S, Jennings G R and Wolf D R 1994 Tomographic reconstruction based on flexible geometric models *Proc. IEEE Int. Conf. on Image Processing (Austin, TX, 1994)* vol II (Los Alamitos, CA: IEEE Computer Society Press) pp 145–7
- Hanson K M, Cunningham G S and McKee R J 1997a Uncertainties in tomographic reconstructions based on deformable models *Proc. SPIE* **3034** 276–86
- 1997b Uncertainty assessment for reconstructions based on deformable models *Int. J. Imaging Systems Technol.* **8** 506–12
- Klein W P, Barrett H H, Pang I W, Patton D D, Rogulski M M, Sain J J and Smith W 1995 FASTSPECT: electrical and mechanical design of a high resolution dynamic SPECT imager *Conf. Record IEEE Nuclear Science Symp. and Medical Imaging Conf. (San Francisco, CA, 1995)* vol II, pp 931–3
- Rossi D J and Willsky A S 1984 Reconstruction from projections based on detection and estimation of objects *IEEE Trans. Acoust. Speech Signal Process.* **32** 886–906
- Shepp L A and Vardi Y 1982 Maximum likelihood reconstruction for emission tomography *IEEE Trans. Med. Imaging* **1** 113–22
- Staib L H and Duncan J S 1996 Model-based deformable surface finding for medical images *IEEE Trans. Med. Imaging* **15** 720–31